AIP | Journal of Applied Physics

Mega-electron-volt proton irradiation on supported and suspended graphene: A Raman spectroscopic layer dependent study

S. Mathew, T. K. Chan, D. Zhan, K. Gopinadhan, A. Roy Barman et al.

Citation: J. Appl. Phys. **110**, 084309 (2011); doi: 10.1063/1.3647781
View online: http://dx.doi.org/10.1063/1.3647781
View Table of Contents: http://jap.aip.org/resource/1/JAPIAU/v110/i8
Published by the American Institute of Physics.

Mega-electron-volt proton irradiation on supported and suspended graphene: A Raman spectroscopic layer dependent study

S. Mathew,[1,a)] T. K. Chan,[2] D. Zhan,[3] K. Gopinadhan,[1,4] A. Roy Barman,[4] M. B. H. Breese,[2] S. Dhar,[1,4] Z. X. Shen,[3] T. Venkatesan,[1,4,b)] and John T. L. Thong[1,c)]
[1]*Department of Electrical and Computer Engineering, National University of Singapore, Singapore 117576*
[2]*Center for Ion Beam Applications (CIBA), Department of Physics, National University of Singapore, Singapore 117542*
[3]*Division of Physics and Applied Physics, School of Physical and Mathematical Sciences, Nanyang Technological University, Singapore 637371*
[4]*NUSNNI-NanoCore, National University of Singapore, Singapore 117576*

(Received 29 July 2011; accepted 30 August 2011; published online 21 October 2011)

Graphene samples with 1, 2, and 4 layers and 1 + 1 folded bi-layers and graphite have been irradiated with 2 MeV protons at fluences ranging from 1×10^{15} to 6×10^{18} ions/cm^2. The samples were characterized using visible and UV Raman spectroscopy and Raman microscopy. The ion-induced defects were found to decrease with increasing number of layers. Graphene samples suspended over etched holes in SiO_2 have been fabricated and used to investigate the influence of the substrate SiO_2 for defect creation in graphene. While Raman vibrational modes at 1460 cm^{-1} and 1555 cm^{-1} have been observed in the visible Raman spectra of substantially damaged graphene samples, these modes were absent in the irradiated-suspended monolayer graphene. © *2011 American Institute of Physics*. [doi:10.1063/1.3647781]

I. INTRODUCTION

Graphene, a two-dimensional (2D) allotrope of carbon where carbon atoms are arranged in a honeycomb structure made out of hexagons, has been the subject of many fascinating studies since its discovery.[1] Its unexpected stability,[2,3] combined with nearly massless behavior of its charge carriers makes it a unique choice for nano-electronic,[4] interconnect,[5] and thermal management applications.[6] For example, high frequency FETs,[7] gas sensors,[8] and solar cells[9] made out of graphene have already been demonstrated.

The ballistic electron transport properties of graphene (mobility$\sim 10^5$ cm^2/V-s) along with its outstanding thermal conductivity ($\sim$5000 W/m/K), the ability of a graphene network to reorganize its structure near a defect site, and the large open space found in between the atomic layers make mono-layer and few-layer graphene an interesting system for ion irradiation studies.[10] Many of the proposed future applications of graphene require controlled introduction of defects into its perfect lattice.[11] Graphene can host lattice defects in reconstructed atom arrangements that do not occur in any other material. It has been shown that energetic particle beams are able to alter the structural, electronic, and magnetic properties of graphite and other carbon allotropes.[12,13] Defects in graphene bring substantial changes near the Fermi level and most of the unique properties of graphene depend on the topology of electronic bands in the vicinity of the Dirac point.[11] Very recently, Chen *et al*. reported Kondo scattering with a gate-tunable Kondo temperature in 500 eV He^+ irradiated monolayer graphene samples.[14] Lattice defects in graphene are a potential source of inter-valley scattering which transforms graphene from a direct-band gap semiconductor to an insulator. The ability of carbon network to induce curvature and also to exist in sp^1-sp^3 hybridizations makes the study of defect-engineering in graphene imperative.

Tapaszto *et al*. reported a reduction in Fermi velocity in 30 keV Ar^+ ion irradiated monolayer graphene using bias dependent STM imaging.[15] Chen *et al*. observed 500 eV He and Ne induced inter-valley scattering and lowering of the minimum conductivity of graphene.[16] Formation of graphene bubbles in graphene with 0.4–0.7 MeV H^+ irradiation has also been reported.[17] Compagini *et al*. investigated 500 keV C^+ irradiation effects in graphene.[18] Very recently, Krasheninnikov and Nordlund reviewed the field of ion and electron irradiation effects in carbon allotropes and other nano-structured materials.[19]

Graphene, being a single atomic layer of carbon atoms, is a unique system to study ion-solid interactions at the beginning of a collision cascade at the microscopic level. The study of the interaction of MeV protons with graphene is stimulated by the potential use of graphene devices in space applications, in particular, graphene based solar cells, which have already been demonstrated.[9] The stability of suspended graphene membranes against energetic ions is of great importance considering the recent work[20] demonstrating graphene as the ultimate membrane for ion-beam analysis of gases and other volatile systems which can not be kept in vacuum. Highly oriented pyrolitic graphite (HOPG) is found to show ferromagnetic ordering when irradiated with MeV protons.[21] Recently, it was shown that 80% of the measured magnetic signal in the 2 MeV H^+ irradiated HOPG originates from the first 10 nm of the surface.[22] This observation indicates that the defects induced by MeV protons in mono-

[a)]Author to whom correspondence should be addressed. Electronic mail: pmsmathew@gmail.com.
[b)]Electronic mail: venky@nus.edu.sg.
[c)]Electronic mail: elettl@nus.edu.sg.

and few-layer graphene play a major role in the reported magnetic ordering of HOPG.

It was believed, based on Mermin-Wagner theorem,[23] that 2D crystals would be structurally unstable due to the long wavelength fluctuations. It has been proposed more recently that corrugations along the third dimension (ripples) in free-standing exfoliated graphene help to make them stable.[2,24] The damage threshold of graphene samples, under MeV proton irradiation, was found to increase with layer number and also when supported by a substrate.[25] In this paper, we concentrate on the evolution of Raman vibrational modes of graphene as a function of graphene layer number and ion fluence and found that supported graphene can accommodate more reconstructions than suspended graphene. Suspended graphene samples were used to probe the role of the SiO_2 substrate for defect creation in graphene.

II. EXPERIMENT

Graphene samples were fabricated using micromechanical exfoliation of Kish graphite and subsequent transfer.[1] The exfoliated graphene flakes were transferred to a silicon piece coated with 280 nm of thermally grown oxide in the case of supported graphene samples. The suspended graphene samples were fabricated by transferring the exfoliated graphene flake onto a SiO_2/Si substrate with an array of pre-patterned holes prepared in the following way. Photolithography was used to transfer the mask pattern consisting of an array of holes into a photo-resist spin coated on SiO_2/Si substrate. This was followed by dry etching of the exposed SiO_2 regions and subsequent removal of the photo-resist. The above substrate was further cleaned using oxygen plasma to remove any residual hydrocarbons remaining on the surface of the substrate. The details of the sample preparation are given in Ref. 25.

One of the inherent technological difficulties in using exfoliated graphene samples for ion irradiation study is the presence of contaminants and adsorbed atoms on the sample, i.e., adhesive tape residues remaining on the sample (both on graphene and on SiO_2) and molecules from the environment adsorbed on the surface of the graphene flake. Moser *et al.* probed the surface of graphene exposed to air and showed that a monolayer of water adsorbs on graphene surface and the adsorbed water does not desorb in vacuum.[26] We designed a two step annealing procedure to realize clean samples for this irradiation study: (a) annealing the exfoliated sample in H_2:Ar (5:95%) at 380 °C for 11 h inside a tube furnace, which is found to be effective in removing the tape residues for the present irradiation study, and (b) heating the sample at 250 °C for 0.50 h inside the irradiation chamber before each irradiation step to remove the adsorbed molecules that had been adsorbed from the ambient air. The pristine samples mentioned in the later part of the text refer to the graphene annealed using step (a) for removing the adhesive tape residues.

Ion irradiations were carried out using a 3.5 MV Singletron facility at the Center for Ion Beam Applications at the National University of Singapore. The graphene samples were loaded into the nuclear microscopy chamber with a strip heater attached in the sample holder for the *in situ* heating procedure mentioned earlier. A collimated beam of 2 MeV protons was focused to a beam spot size of $\sim 5\,\mu$m on target using a set of quadrupole lenses. An optical microscope attached to the irradiation chamber was used to locate the graphene flake in the sample. The focused ion beam was then raster-scanned under normal incidence over an area of $800 \times 800\,\mu m^2$ with the graphene flake positioned at the centre of each scan. The pressure in the chamber during the irradiation was 1×10^{-6} mbar. The ion beam current density was kept at $0.5\,pA/\mu m^2$ for ion fluences up to 1×10^{18} ions/cm^2, and $1.3\,pA/\mu m^2$ for ion fluences 6×10^{18} ions/cm^2 and above. Visible Raman spectroscopy and imaging were carried out using a WITec CRM200 Raman system. The excitation wavelength used was 532 nm, and the laser power at the sample was below 0.5 mW/cm^2 to avoid laser induced heating. Raman microscopy was done using a x-y piezo-stage. A 100× objective lens was used with a laser spot size of ~ 600 nm. The stage movement and data acquisition were controlled using ScanCtrl Spectroscopy Plus software from WITec GmbH. A Renishaw Invia spectrometer was used for ultraviolet Raman spectroscopy measurements. The wavelength used was 325 nm with an intensity of 5 mW/cm^2 at the source. A 40× objective lens with a numerical aperture of 0.5 was used. The Raman spectrum was analysed by curve fitting using multiple Lorentzians with a slopping background.

III. RESULTS AND DISCUSSION

The Raman spectrum of a pristine monolayer graphene flake is shown in Fig. 1(a). The prominent Raman modes in Fig. 1(a) are at 1602 cm^{-1} and 2694 cm^{-1}. The mode at 1602 cm^{-1} is the G mode due to the in-plane bond stretching motion of the pairs of carbon atoms with E_{2g} symmetry. This is associated with the zone center longitudinal optical (LO) phonons. The mode at 2694 cm^{-1} is the 2D mode which originates from a double resonance process consisting of inelastic-scattering events involving two phonons with opposite momenta.[27] The other modes in Fig. 1(a) are the one at

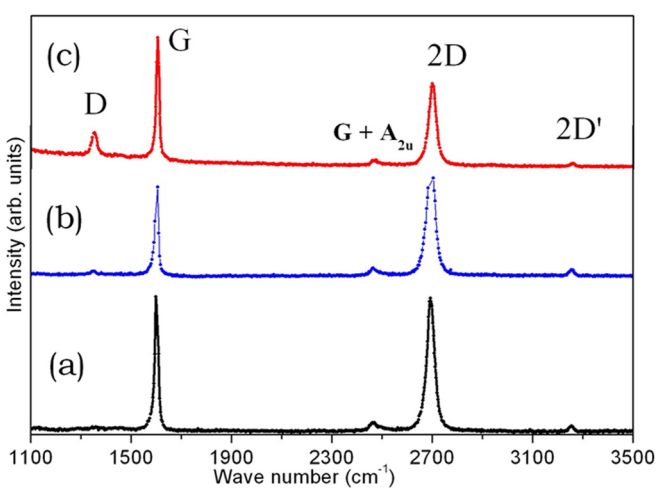

FIG. 1. (Color online) Raman spectrum from a (a) pristine monolayer graphene and irradiated monolayer graphene at fluences of (b) 1×10^{15} ions/cm^2 and (c) 1×10^{16} ions/cm^2. Threshold fluence for observation of ion damage is $\sim 1 \times 10^{16}$ ions/cm^2.

2467 cm^{-1}, which is a combination mode of G and A_{2u} vibrations, and another at 3250 cm^{-1} being the second order mode of D′, which will be explained in the later part of the article. The FWHM of the 2D peak is 33 cm^{-1} which corresponds to a monolayer graphene.[28]

For an electrically neutral graphene sample the position of the G, 2D peaks will be at $\sim$1580 cm^{-1} and 2670 cm^{-1}, respectively.[27] A blue shift of the above peaks and a reduction in the intensity of 2D peak in annealed and air exposed graphene samples is a common feature due to the intrinsic hole doping effect from the ambient air, as reported by Ni *et al.*[29] In Ref. 29, when the annealed and air-exposed graphene samples were again heated in vacuum, Raman spectra were found to retrace back to the pristine graphene, i.e., the adsorbents had been effectively removed.

The threshold ion fluence required for an observable defect in monolayer has been investigated before starting a systematic study of ion irradiation. Monolayer graphene areas irradiated at fluence of 1×10^{15} and 1×10^{16} ions/cm^2 are shown in Figs. 1(b) and 1(c), respectively. Apart from the aforementioned Raman peaks, a mode at 1352 cm^{-1}, called D peak, is also visible in Figs. 1(b) and 1(c). This is the in-plane breathing mode of A_{1g} symmetry due to the presence of six-fold aromatic rings and requires a defect for its activation. The D peak comes from the in-plane transverse optic (TO) phonons around the **K** point of the Brillouin zone and is strongly dispersive due to Kohn anomaly at **K**.[27] In Fig. 1(b), the D peak is barely visible and the integrated intensity ratio of D to that of G (denoted as I(D)/I(G)) is 0.03, while in Fig. 1(c) it has become 0.34. From Fig. 1, it is clear that the threshold ion fluence for the creation of defects detectable by Raman spectroscopy in monolayer graphene is $\sim 1 \times 10^{16}$ ions/cm^2.

We have used a graphene sample with a region encompassing 1, 2, 4 layers and a 1 + 1 folded bi-layer region to study the effects of MeV proton irradiation. The same sample was irradiated subsequently to probe the ion fluence variation. An optical micrograph of the sample is shown in Fig. 2(a), where the different optical contrasts indicate different layer numbers. Further, the layer thickness and uniformity have been confirmed by using Raman imaging of the above flake. The differences in layer numbers are clear from the Raman image using the FWHM of the 2D band shown in Fig. 2(b).

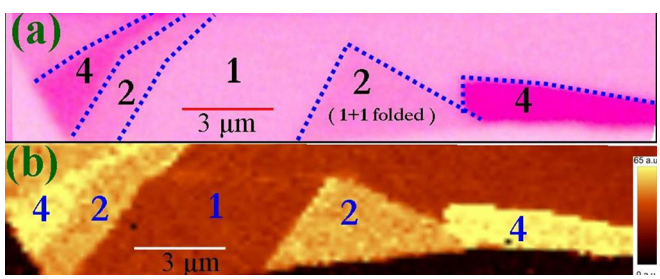

FIG. 2. (Color online) (a) Optical micrograph of the graphene flake with 1, 2, 4, and a 1 + 1 folded graphene layers. (b) The corresponding Raman microscopy image using the FWHM of 2D peak. The graphene layer numbers are labeled in both (a) and (b).

The above graphene sample was irradiated at fluences 1×10^{17}, 1×10^{18}, and 6×10^{18} ions/cm^2. Raman imaging and spectroscopy were done on every fluence, and the I(D)/I(G) ratio was computed using the integrated intensities of D and G peaks. The intensities of I(D)/I(G) ratio of the irradiated samples are shown in Figs. 3(a)–3(c). The enhanced colour contrasts in Figs. 3(a) and 3(b) for monolayer indicate that the induced defects in monolayer are higher than those of few-layer graphene. In Fig. 3(c), at a fluence of 6×10^{18} ions/cm^2, graphene has been damaged substantially, and the layer contrasts are not obvious. The Raman micrograph in Fig. 3 shows that the induced defects in various layers are uniform. To understand the microscopic nature of damage, the Raman spectrum of each layer was analysed.

Raman spectra of pristine and irradiated monolayer graphene are shown in Figs. 4A(a)–(d). The G, 2D modes at 1587 cm^{-1} and 2669 cm^{-1} are clearly visible in the pristine spectra. On the irradiated samples, apart from G, 2D modes and a peak at $\sim$1350 cm^{-1} which is the D mode, another peak at 2930 cm^{-1} which is a combination mode of D and G is clearly visible.[27,30] As the fluence increases, the second order peaks are getting wider and in Fig. 4A(d) those peaks are barely seen. The deconvolution of the spectrum in the irradiated samples in panels (e)–(h) shows a sharp mode at 1623 cm^{-1} called the D′ mode and extra broad features at 1460 cm^{-1} and 1555 cm^{-1}. The D′ mode is due to an intravalley double resonance process at **K** point involving a single phonon and a defect [27]. The possible origins of the features at 1460 cm^{-1} and 1555 cm^{-1} will be discussed in the later part of this article. As the ion fluence increases, I(D)/I(G) is found to be increasing and the width of the D peak has increased from 33 cm^{-1} at a fluence of 1×10^{18} ions/cm^2 to 117 cm^{-1} in the sample irradiated at a fluence of 6×10^{18} ions/cm^2. A minor red shift ($\sim$4 cm^{-1}) in the peak position of the D mode is visible in Fig. 4A(d) in comparison with Fig. 4A(b). Compagini *et al.* also observed similar red shifts of D peak in keV carbon irradiated monolayer graphene.[18] The intensity of the D′ mode is also found to increase with ion fluence. The shape of the spectra around the D peak indicates that the broad features at 1460 cm^{-1} and 1555 cm^{-1} are getting enhanced with I(D)/I(G) ratio,

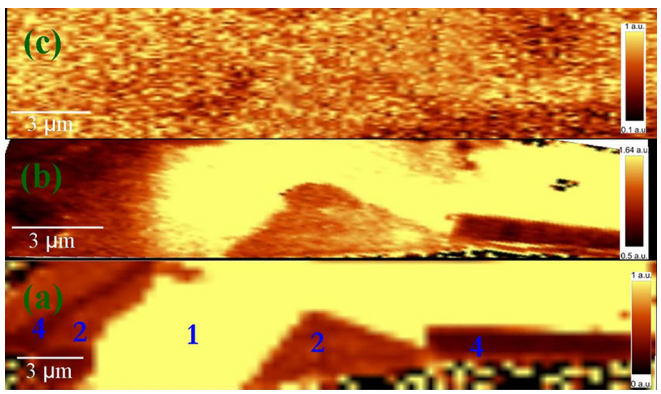

FIG. 3. (Color online) Raman microscopy image created using the I(D)/I(G) ratio of the graphene sample in Fig. 2 irradiated at fluence of (a) 1×10^{17} ions/cm^2, (b) 1×10^{18} ions/cm^2, and (c) 6×10^{18} ions/cm^2, respectively. The layer numbers are indicated in (a). (The colour contrast is enhanced in all the panels.)

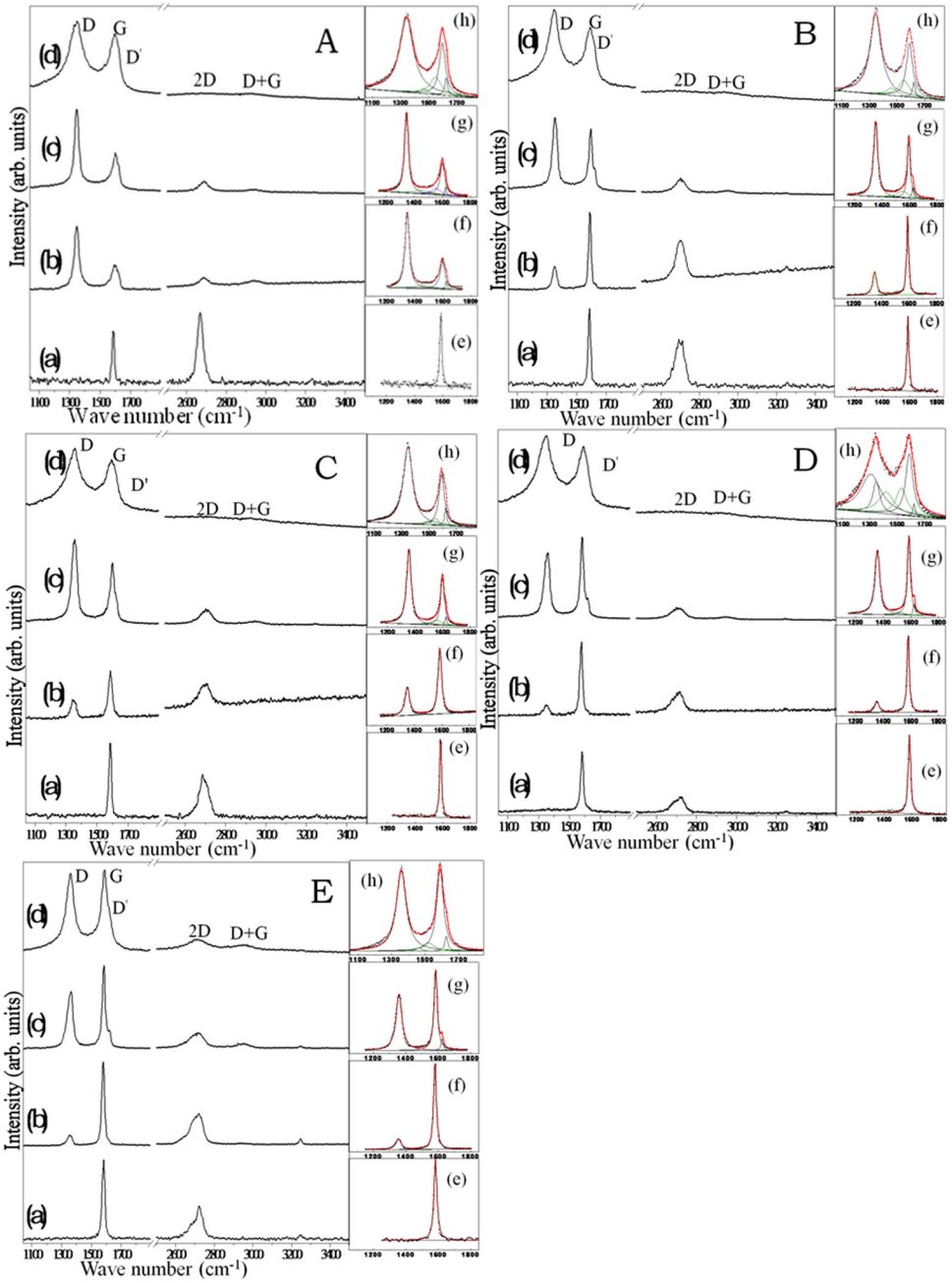

FIG. 4. (Color online) Panel A—Raman spectrum from (a) pristine monolayer graphene and the same sample irradiated at fluences of (b) 1×10^{17} ions/cm^2, (c) 1×10^{18} ions/cm^2, and (d) 6×10^{18} ions/cm^2; the corresponding fitted curve with constituent peaks and experimental points are shown in (e)–(h). Panels (B)–(E) correspond to the same for a 2 layer graphene, folded $1+1$ graphene, 4-layer graphene, and graphite, respectively.

and the total intensity of these two peaks became 70% of the G mode in Fig. 4A(d).

Raman spectra of the pristine and irradiated bi-layer and $1+1$ folded graphene are shown in Figs. 4B and 4C. Ni *et al*. reported a sharp 2D band with FWHM similar to that of a monolayer graphene for a $1+1$ folded bi-layer graphene.[31] A reduction in the Fermi velocity has also been attributed to the monolayer-like electronic structure of folded graphene in Ref. 31. We have not observed a similar behavior in the FWHM of 2D peak in our sample. The FWHM of the 2D peak in Fig. 4C(a) is comparable to that of the bi-layer graphene in Fig. 4B(a), which is also clear from the Raman image shown in Fig. 3(b). The FWHM of 2D peak in monolayer, folded region, and bi-layer on our sample are 33, 52, 54 cm^{-1}, respectively. One of the reasons behind the enhanced FWHM of the 2D peak in the folded region may be the healing of the rotational disorder present in the sample due to an annealing process. Further experiments on folded and annealed graphene samples are required uncover the reason behind this observation.

The Raman spectra of irradiated bi-layer graphene and folded graphene region are shown in Figs. 4B(b)–(d) and 4C(b)–(d). The D peak starts to appear at a fluence of 1×10^{17} ions/cm^2 with I(D)/I(G) ratio of ~ 0.5 in both of the spectra and this ratio is found to increase with fluence. The width of the D peak is ~ 40 cm^{-1} in Figs. 4C(b) and (c) while it is 32 cm^{-1}, and 40 cm^{-1}, respectively, in Figs. 4B(b) and (c) in the bi-layer sample. The D peak has widened at a fluence of 6×10^{18} ions/cm^2 and become 82 cm^{-1} and 97 cm^{-1} in folded and bi-layer graphene samples. The features around 1460 cm^{-1} and 1555 cm^{-1} and the D′ peak start to appear only at a fluence of 1×10^{18} ions/cm^2 in both of the above

samples where I(D)/I(G) ratio has became 2. In Figs. 4C(h) and 4B(h), at the highest fluence, the total intensity of the broad features observed in between D and G peaks became 27% of G peak in the folded region, while it became 73% of the G peak in the bi-layer sample.

Figs. 4D and 4E show the Raman spectra of pristine and irradiated 4-layer graphene and graphite samples. A D peak with 26% intensity of G peak is visible in Fig. 4D(b), and the peak intensity has been increasing with fluence. In Fig. 4D(d), the D peak is found to be highly asymmetric, a broad band at 1311 cm^{-1} is clear from the fitted data in the inset. The broad modes at 1460 cm^{-1} and 1555 cm^{-1} start to appear at a fluence of 1×10^{18} ions/cm^2, where I(D)/I(G) ratio is 1.31 and the total intensity of these modes are comparable to that of G mode in Fig. 4D(d). A low intensity D′ mode is present in Figs. 4D(c) and (d). The graphite sample shows a D mode with 23% intensity of G mode in Fig. 4E(b), and the I(D)/I(G) ratio has become 1.4 in the sample irradiated at a fluence of 6×10^{18} ions/cm^2. The modes at 1460 cm^{-1} and 1555 cm^{-1} have appeared only in Fig. 4E(d), and the total intensity of these modes is 20% of that of G mode. A low intensity D′ mode can be seen in Figs. 4E(c) and (d).

The ability of the carbon network to reorganize a vacancy site points towards the possibility of non-hexagonal rings and thus the formation of C-C σ bonds.[3,10] The bridging of graphene planes by C-C σ bonds due to the defects produced by ion or electron irradiation has been also demonstrated.[10,32] Visible Raman spectroscopy is 50–230 times more sensitive to sp^2 sites compared to sp^3 sites as visible photons preferentially excite the π-states (exciting σ states of the sp^3 sites require higher photon energy).[33] We have carried out UV-Raman spectroscopy on the irradiated samples to check the formation of sp^3 hybridization and calculate the dispersion of the D, 2D modes.

The UV Raman spectra of the irradiated monolayer, bilayer graphene and graphite, using 325 nm as the excitation radiation are shown in Fig. 5. The D, 2D peaks are found to be shifted to higher wave numbers compared to visible Raman spectra. The zone center G mode has not shown any dispersion with excitation wavelength. The intensities of the D, 2D peaks were reduced in the UV Raman spectra. Very recently, Calizo *et al.* reported the UV Raman spectra of pristine graphene.[34] A reduction in the intensity of the D, 2D peaks with an increase in the excitation radiation in the case of reduced graphene oxide has been recently reported by Zhan *et al.*[31] The width of the D peak in all of the spectra (Fig. 5) is found to be double that observed using the visible excitation: in the case of substantially damaged monolayer at the highest fluence, the FWHM of D peak in Fig. 5A(c) is 117% of that of visible spectra. The D peak starts to appear at a fluence of 1×10^{18} ions/cm^2 in bi-layer, 4-layer, and graphite, whereas in monolayer graphene it is present in all of the spectra as shown in Fig. 5. In graphite, at a fluence of 1×10^{19} ions/cm^2, peaks are also visible at 1837 cm^{-1} and 3158 cm^{-1}. The first peak can be due to the presence of linear carbon chains as reported by Scuderi *et al.*[35] The second peak position is close to the second order mode of G peak. Ravindran *et al.* observed a mode at 3150 cm^{-1} in the UV Raman spectrum of single walled carbon nanotube and assigned this peak to the second order of the G mode.[36] In all of the above spectra, another important feature is the absence of the broad peaks around 1460 cm^{-1} and 1555 cm^{-1} observed in the deconvoluted spectra of the visible Raman spectra in Fig. 4.

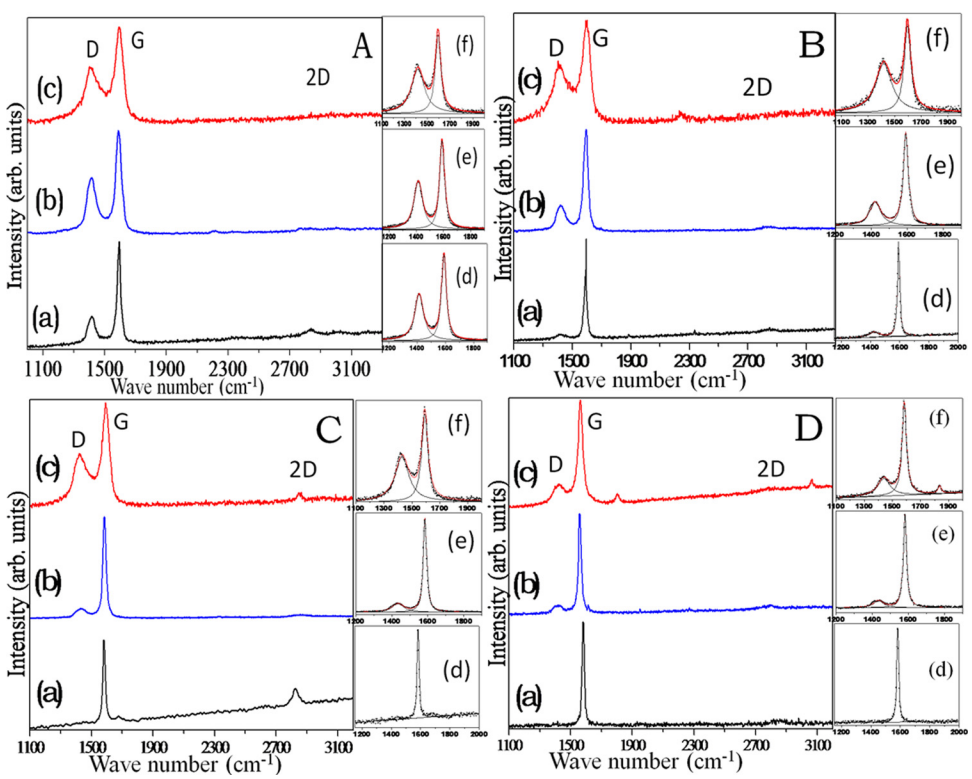

FIG. 5. (Color online) Panel-A—UV Raman spectrum from (a) a pristine monolayer graphene and irradiated graphene at fluences of (b) 1×10^{17} ions/cm^2, (c) 1×10^{18} ions/cm^2, and (d) 6×10^{18} ions/cm^2; the fitted spectrum with constituent peaks and experimental points are shown in (d)–(f). Panels (B)–(D) correspond to the same for a 2-layer, 4-layer, and graphite samples.

The ion induced damage in monolayer graphene is found to be more than that of multi-layer at all of the ion fluences and it starts to grow in a non-linear fashion (Fig. 4). The appearance of the broad features in between D and G peaks in monolayer and the double peak structure of the D mode in the 4-layer sample in Fig. 4D(d) indicate that these modes may arise from interlayer interactions, both graphene-graphene and/or graphene-SiO_2. The appearance of enhanced damage in monolayer compared to multi-layers can also be due to interaction of graphene with the underlying substrate SiO_2. We have fabricated a suspended sample with one and three layer graphene to investigate the effect of substrate SiO_2 for defect creation in graphene.

An optical micrograph of the suspended graphene samples is shown in Figs. 6(a) and 6(c), respectively. The suspended graphene regions are indicated using arrows. One of the ways to check whether a graphene flake remains free-standing is by comparing the intensity of 2D peak (I(2D)) to that of G peak (I(G)) of the Raman spectrum.[37] Raman microscopy images showing the I(2D)/I(G) ratio of monolayer and 3-layer regions are given in Figs. 6(b) and 6(d). The intense signal (from the colour code) in Figs. 6(b) and 6(d) at the suspended region shows that the graphenes remain free-standing over the etched hole in SiO_2. Conventionally, a reduction in the intensity of Raman modes in a suspended region is expected because of the interference enhancement of the signal in the supported graphene region, and the G mode agrees with the above.[38] The 2D mode intensity is found to be enhanced in the suspended region. It has been shown that the intensity of 2D mode is proportional to the inverse of the inelastic scattering rate and which in turn depends on the amount of charged impurities present in graphene flake.[37] On the suspended region, the intrinsic charged impurity doping from the substrate is absent, and hence, the 2D mode has enhanced intensity compared to supported graphene.[37] The I(2D)/I(G) ratio can be used to estimate the amount of charged impurities. In Fig. 6(b) in the monolayer suspended region this ratio is 8.4 and which corresponds to

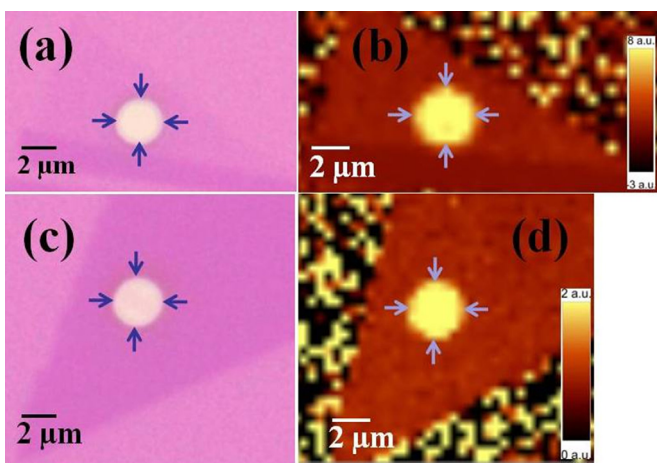

FIG. 6. (Color online) Optical micrograph of suspended (a) monolayer graphene sample and (c) three layer graphene sample. The corresponding Raman Microscopy image created using the I(2D)/I(G) ratio of (b) monolayer, (d) 3-layer graphene sample. The suspended graphene region is indicated using arrows in all the panels.

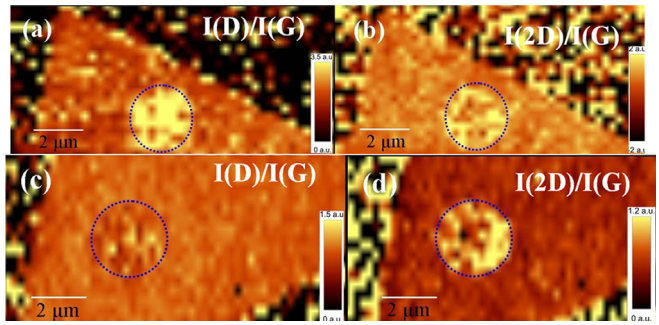

FIG. 7. (Color online) Raman microscopy image of the graphene sample in Fig. 6 irradiated at a fluence of 1×10^{18} ions/cm^2. The I(D)/I(G) ratio and the I(2D)/I(G) ratio of the suspended monolayer graphene sample is given in panels (a) and (b), respectively. Panels (c) and (d) correspond to the same for a 3-layer suspended graphene sample. The suspended graphene region is marked using a dashed circle.

an intrinsic doping $< 10^{12}$ atoms/cm^2, while at the supported region the ratio is 3.3, which corresponds to a doping level of 4×10^{12} atoms/cm^2.[37]

The I(D)/I(G) and I(2D)/I(G) images of the irradiated suspended monolayer and 3-layer graphene samples at fluences of 1×10^{18} and 1×10^{19} ions/cm^2 are shown in Figs. 7 and 8. It can be seen that the induced defects in the suspended monolayer region are higher than those of the supported region in Fig 7(a), while in Fig. 7(c), the signal intensity is uniform throughout the sample. This indicates that the induced defects in supported and suspended regions of the tri-layer sample are of same amount. The enhanced signal intensity at the suspended region in Figs. 7(b) and 7(d) indicates that the graphene flakes remain suspended in both one and three layer samples even after irradiating with 1×10^{18} ions/cm^2. On the sample irradiated at 1×10^{19} ions/cm^2, the defects are found to be uniform in both in 1, 3-layer samples (Figs. 8(a) and 8(c)). The I(2D)/I(G) ratio shows that 3-layer graphene remains suspended, while the signal intensity at the suspended region of the monolayer has been diminished considerably and it appears to have fallen into the etched hole below. The AFM results (not shown here) on the sample irradiated at a fluence of 1×10^{19} ions/cm^2 show that the 3-layer graphene

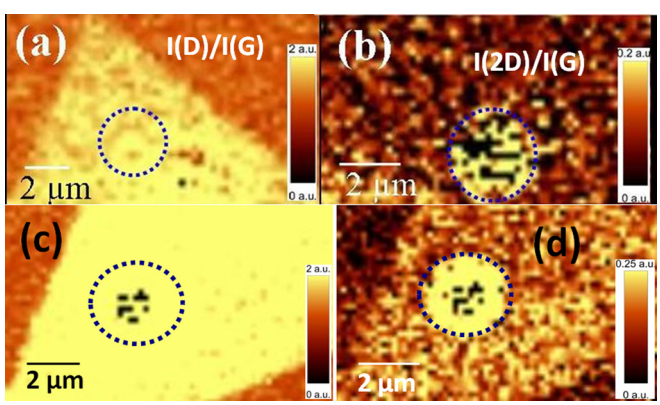

FIG. 8. (Color online) Raman microscopy image of the graphene sample in Fig. 6 irradiated at a fluence of 1×10^{19} ions/cm^2. The I(D)/I(G) ratio and the I(2D)/I(G) ratio of the suspended monolayer graphene sample is given in panels (a) and (b) respectively. Panels (c) and (d) corresponds to the same for a three layer suspended graphene sample. The suspended graphene region is marked using a dashed circle.

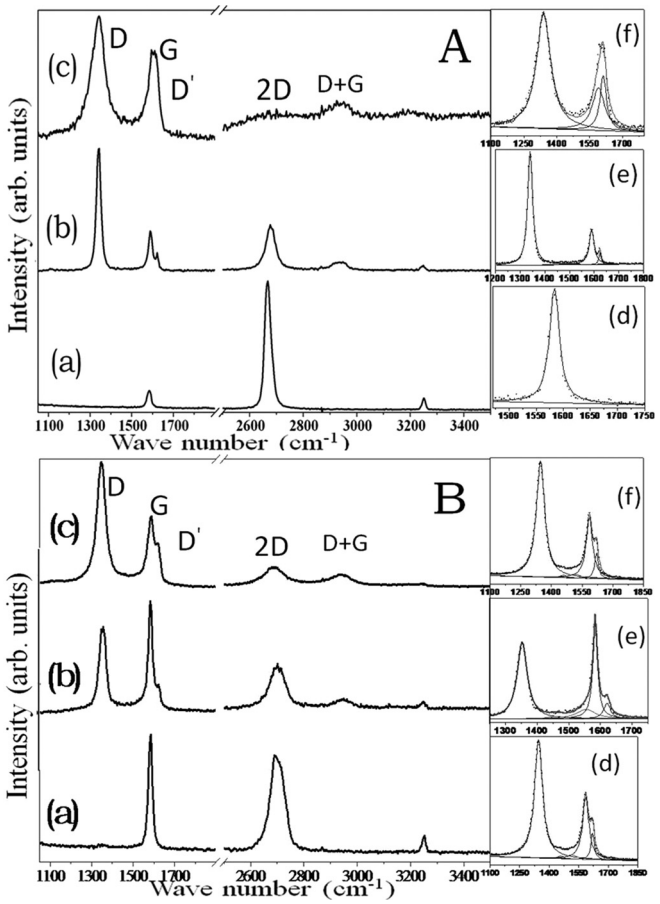

FIG. 9. Panel-A—Raman spectrum from a (a) pristine monolayer suspended graphene and irradiated monolayer suspended graphene at fluences of (b) 1×10^{18} ions/cm^2 and (c) 1×10^{19} ions/cm^2; the fitted spectrum with constituent peaks are shown in (d)–(f). Panel B corresponds to the same for a 3-layer suspended graphene sample.

remains suspended while the monolayer has collapsed into the etched hole.[25]

The Raman spectra of the pristine and irradiated suspended monolayer, 3-layer samples are shown in Figs. 9(A) and 9(B), respectively. The FWHM of the 2D peak in the pristine samples are 26, 59 cm^{-1}, respectively, and which corresponds to mono and ~3-layer graphene.[28] The absence of the broad features at 1460 cm^{-1} and 1555 cm^{-1} in the monolayer suspended graphene is clear from Fig. 9(A), while in the 3-layer sample in Fig. 9(B), the shape of the spectra in between D and G region indicate that those peaks are required to get a better fit of the experimental data. The intensity of these peaks in the supported graphene (not shown here) is found to be more than that of suspended region. A double peak structure of the D peak, similar to 4-layer graphene in Fig. 4(C), was also observed in supported 3-layer sample. Another important feature in the suspended graphene is the appearance of a strong D′ peak compared to that in supported region; in monolayer, at a fluence of 1×10^{19} ions/cm^2 it has become 70% of the G mode. This indicates strong intra-valley scattering at the suspended region in comparison with supported region.

The broad features at 1460 cm^{-1} and 1555 cm^{-1} start to appear in monolayer graphene at a fluence of 1×10^{17} ions/cm^2, bi-layer and 4-layer at 1×10^{18} ions/cm^2, and in the graphite at a fluence of 6×10^{18} ions/cm^2. These modes have not been observed in any of the irradiated suspended monolayer samples. Raman modes at these positions have been reported in 3D graphene systems and diamond-like carbon films.[39] We have observed that these peaks require certain threshold defect density for activation (mono- and few-layer graphene I(D)/I(G) ratio of ~2 and in graphite ~1.3). These modes were completely suppressed in the UV Raman spectra of supported samples. Doyle and Dennison estimated the Raman vibrational modes of non-Benzene-ring structures and assigned peaks at 1444 cm^{-1} and 1529 cm^{-1} for a five member carbon ring structure.[40] The observed broad features in between D and G regions are close to the calculated vibrational modes of a five member ring structure. The absence of these modes in suspended monolayer indicates that the origin of this can be due to inter-layer interactions—graphene-graphene and graphene with substrate SiO_2. The induced defects in monolayer suspended graphene are found to be more than those of supported graphene in Fig. 7(a) at a fluence of 1×10^{18} ions/cm^2, while it has collapsed into the etched hole at a fluence of 1×10^{19} ions/cm^2 [Fig. 8(a)]. The 3-layer graphene remains suspended at the highest fluence and the healing of the defects in multi-layer graphene can be either due to the formation of non-six member ring structures or inter-layer sp^3 bond formation. The UV Raman results in Fig. 5 do not show the formation of inter-layer diamond-like bond implying post-irradiation reconstruction to be restricted to the planes. Monolayer suspended graphene disintegrates at a fluence of 1×10^{19} ions/cm^2 and is no longer suspended. The most probable defects in graphene are atomic vacancies and Stone-Wales defects.[41] The ability of C-C bond to reconstruct at a vacancy site and to form a coherent defective lattice without under-coordinated atoms is a unique feature of the graphene lattice. This indicates that the ability of a suspended monolayer graphene to reconstruct its lattice and repair the induced defects is weak compared to supported graphene (either by another graphene layer or by substrate SiO_2) samples. The absence of broad features at 1460 cm^{-1} and 1555 cm^{-1} in suspended monolayer along with the absence of inter-layer diamond-like bond in the irradiated supported graphene samples indicates that the interaction between graphene-graphene and graphene with SiO_2 is important for the reconstruction of graphene lattice to form pentagons and other non-six member ring structures.

Assuming a linear dispersion relation for the D, 2D peaks, for 325 and 532 nm excitation, we calculated the dispersion for D, 2D modes which are shown in Table I. Thomson and Reich reported a frequency shift of 60 cm^{-1}/eV for the D mode in graphite.[42] Recently, Narula and Reich reported the quenching of the D mode intensity with increasing excitation radiation and predicted a smaller value of the D mode dispersion in graphene compared to that of the graphite D mode for excitation energies in 2–3 eV range.[43] Our results (from Table I) show a dispersion of~ 48 cm^{-1}/eV for graphene, which is smaller than the dispersion values of few-layer graphene and graphite. Also we observed a decrease of the D mode intensity in the UV Raman spectra in Fig. 5 compared to that in the visible Raman spectra (Fig. 4). The dispersion obtained for 2D mode is roughly double that

TABLE I. The dispersion of D and 2D peaks in cm^{-1}/eV calculated using 532 nm and 325 nm excitations.

	1 Layer		2 Layer		4 Layer		Graphite	
Fluence (ions/cm^2)	D	2D	D	2D	D	2D	D	2D
1×10^{17}	47	99	51	100	–	–	–	–
1×10^{18}	47	77	46	87	52	107	51	108
6×10^{18}	51	–	48	–	55	110	56	116

of the D peak (Table I) and is expected for a double resonance process.

The induced damage in monolayer is found to be higher in all the 3 ion fluences used in this work. These results in conjunction with the observation of higher I(D)/I(G) ratio in the suspended monolayer compared to supported region clearly demonstrate that the graphene-graphene interaction along the third dimension makes the quasi two dimensional graphene more stable.

The electronic and the nuclear energy loss of 2 MeV H^+ ions in an amorphous carbon target with the density of graphite is estimated (using SRIM[44]) to be 3.2 eV/Å and 2×10^{-3} eV/Å respectively. The displacement per atom (dpa) for 2 MeV protons at a fluence of 1×10^{17} ions/cm^2 is 0.0004. The above factor is based on Ziegler-Biersack-Littmark (ZBL) theory of ion stopping[44] and cannot explain the nature of the observed damage and the quenching of the defects with layer number. Production of defects in nano-systems is different from that in bulk materials. The system dimensions and size significantly affect the dissipation of energy brought in by the energetic particle.[19] A model of intense electronically stimulated surface desorption of the atoms has been found to be appropriate in the damage creation of MeV protons in graphene.[25]

IV. CONCLUSION

A systematic study of the interaction of 2 MeV protons with mono and few-layer graphene has been carried out. The threshold ion fluence to create an observable damage in monolayer graphene is found to be $\sim 1 \times 10^{16}$ ions/cm^2. The stability of graphene is found to increase with increasing layer number - this points towards the role of interaction along the third dimension in stabilizing the quasi two-dimensional graphene. The induced defects were found to grow in a non-linear fashion with ion fluence. Broad peaks at 1460 cm^{-1} and 1555 cm^{-1} start to appear in the Raman spectra of most of the irradiated samples when the intensity of D peak becomes comparable to the G peak, while these features were not observed in suspended monolayer graphene. This implies that the suspended monolayer graphene samples may not be able to support a non-six-fold ring structures compared to multi-layer graphene or graphene supported by a substrate. UV Raman spectra have not shown modes corresponding to diamond-like bonding in the irradiated graphene samples and possibly the post damage reconstruction to be restricted to the planes.

ACKNOWLEDGMENTS

We acknowledge Professor Ting Yu and Ms. Yanan Xu (Division of Physics and Applied Physics, NTU, Singapore) for their help in Raman spectroscopy measurements. S. Mathew would like to acknowledge Mr. Shawn Lee Ken Seng (WITec, Singapore) for some of the Raman Microscopy experiments. This work was funded by an NRF-CRP grant on "Graphene Related Materials and Devices."

[1] K. S. Novoselov, A. K. Geim, S. V. Morozov, D. Jiang, Y. Zhang, S. V. Dubonos, I. V. Crigorieva, and A. A. Firsov, Science **306**, 666 (2004).
[2] K. S. Novoselov, D. Jiang, F. Schedin, T. J. Booth, V. V. Khotkevich, S. V. Morozov, and A. K. Geim, Proc. Natl. Acad. Sci. USA **102**, 10451 (2007).
[3] M. H. Gass, U. Bangert, A. L. Bleloch, P. Wang, R. R. Nair, and A. K. Geim. Nat. Nanotech. 2578 (2011).
[4] M. Annamalai, S. Mathew, V. Viswanathan, C. Fang, D. S. Pickard, and M. Palaniapan, Solid-State Sensors, Actuators and Microsystems Conference (TRANSDUCERS), 2578 (2011).
[5] R. Murali, Y. Yang, K. Brenner, T. Beck, and J. D. Meindl, Appl. Phys. Lett. **94**, 243114 (2009).
[6] S. Ghosh, I. Calizo, D. Teweldebrhan, E. P. Pokatilov, D. L. Nika, and A. A. Balandin, Appl. Phys. Lett. **92**, 151911 (2008).
[7] F. Xia, D. B. Farmer, Y. Lin, and P. Avouris, Nano Lett. **9**, 422 (2009).
[8] A. Ghosh, D. J. Late, L. S. Panchakarla, A. Govindaraj, and C. N. R. Rao, J. Exp. Nanosci. **4**, 313 (2009).
[9] X. Li, H. Zhu, K. Wang, A. Cao, J. Wei, C. Li C, Y. Jia, Z. Li, X. Li, and D. Wu, Adv. Mater. **22**, 2743 (2010).
[10] A. Krasheninnikov and F. Banhart, Nature Mater. **6**, 723 (2007).
[11] L. D. Carr and M. T. Lusk, Nat. Nanotech. **5**, 316 (2010).
[12] V. M. Pereria, J. M. B. Lopes dos Santos, and A. H. Castro Neto. Phys. Rev. B **77**, 115109 (2008).
[13] S. Mathew S. B. Satpati, B. Joseph, B. N. Dev, R. Nirmala, S. K. Mallik, and R. Kesavamoorthy, Phys. Rev. B **75**, 75426 (2007).
[14] J. H. Chen, L. Li, W. G. Cullen, E. D. Williams, and M. F. Fuhrer, Nature Phys. **7**, 535 (2011).
[15] L. Tapaszto, G. Dobrik, P. Nemes-Incze, G. Vertesy, P. H. Lambin, and L. P. Biro, Phys. Rev. B **78**, 233407 (2008).
[16] J. H. Chen, W. G. Cullen, E. D. Williams, and M. F. Fuhrer, Phys. Rev. Lett. **102**, 236805 (2009).
[17] E. Stolyarova, D. Stolyarov, K. S. Bolotin, S. Ryu, L. Liu, K. T. Rim, M. Klima, M. Hybertsen, I. Pogorelsky, I. Pavlishin, K. Kusche, J. Hone, P. Kim, H. L. Stormer, V. Yakimenko, and G. Flynn, Nano Lett. **9**, 332 (2009).
[18] G. Compagnini, F. Giannazzo, S. Sonde, V. Raineri, R. Rimini, and E. Rimini, Carbon **47**, 3201 (2009).
[19] A. V. Krasheninnikov and K. Nordlund, J. Appl. Phys. **107**, 71301 (2010).
[20] O. Lehtinen, J. Kotakoski, A. V. Krasheninnikov, A. Tolvanen, K. Nordlund, and J. Keinonen, Phys. Rev. B **81**, 153401 (2010).
[21] M. A. Ramos, J. Barzola-Quiquia, P. Esquinazi, A. Muñoz-Martin, A. Climent-Font, and M. García-Hernández, Phys. Rev. B **81**, 214404 (2010).
[22] H. Ohldag, P. Esquinazi, E. Arenholz, D. Spemann, M. Rothermel, and A. Setzer, New. J. Phys. **12**, 123012 (2010).
[23] N. D. Mermin, Phys. Rev. B **176**, 250 (1968).
[24] A. Fasolino, J. H. Los, and M. I. Katsnelson, Nature Mater. **6**, 858 (2007).
[25] S. Mathew, T. K. Chan, D. Zhan, K. Gopinadhan, A. R. Barman, M. B. H. Breese, S. Dhar, Z. X. Shen, T. Venkatesan, and John T. L. Thong, Carbon **49**, 1720 (2011).
[26] J. Moser, A. Verdaguer, D. Jimenez, A. Barreiro, and A. Bachtold, Appl. Phys. Lett. **92**, 123507 (2008).
[27] D. M. Basco, S. Piscanec, and A. C. Ferrari, Phys. Rev. B. **80**, 165413 (2009); A. C. Ferrari, J. C. Meyer, V. Scardaci, C. Casiraghi, M. Lazzeri, F. Mauri, S. Piscanec, D. Jiang, K. S. Novoselov, S. Roth, and A. K. Geim, Phys. Rev. Lett. **97**, 187401 (2006).
[28] Y. Hao, Y. Wang, L. Wang, Z. H. Ni, Z. Wang, R. Wang, C. K. Koo, Z. X. Shen, and John T. L. Thong, Small **195**, 99 (2009).
[29] Z. H. Ni, H. M. Wang, Z. Q. Luo, Y. Y. Wang, T. Yu, Y. H. Wu, Z. X. Shen, Z. X. Shen, J. Raman Spectrosc. **41**, 479 (2009).
[30] D. Zhan, Z. H. Ni, W. Chen, L. Sun, Z. Luo, L. Lai, T. Yu, A. T. S. Wee, and Z. X. Shen, Carbon **49**, 1362 (2011).
[31] Z. H. Ni, Y. Y. Wang, T. Yu, Y. M. You, and Z. X. Shen, Phys. Rev. B **77**, 235403 (2008).
[32] R. H. Telling, C. P. Ewels, A. A. El-Barbary, and M. I. Heggie, Nature Mater. **2**, 333 (2003).
[33] A. C. Ferrari and J. Robertson, Phys. Rev. B **61**, 14095 (2000).

[34]I. Calizo, I. Bejenari, M. Rahman, G. Liu, and A. A. Balandin, J. Appl. Phys. **106**, 43509 (2009).
[35]V. Scuderi, S. Scalese, S. Bagiante, G. Compagnini, L. D′Urso, and V. Privitera, Carbon **47**, 2134 (2009); L. D′Urso, G. Compagnini, O. Puglisi, *ibid*. **44**, 2093 (2006); X. Zhao Y. Ando, Y. Liu, M. Jinno, and T. Suzuki, Phy. Rev. Lett. **90**, 187401 (2003).
[36]T. R. Ravindran, B. R. Jackson, and J. V. Baddling, Chem. Mater. **13**, 4187 (2001).
[37]Z. H. Ni, T. Yu, Z. G. Luo, Y. Y. Wang, L. Liu, C. P. Wong, J. Miao, W. Huang, and Z. X. Shen, ACS Nano **3**, 569 (2009); S. Berciaud, S. Ryu, L. E. Brus, and T. F. Heinz, Nano Lett. **9**, 346 (2009).
[38]Y. Y. Wang, Z. H. Ni, Z. X. Shen, H. M. Wang, and Y. H. Wu, Appl. Phys. Lett. **92**, 43121 (2008).
[39]S. Mathew, U. M. Bhatta, J. Ghatak, B. R. Sekhar, and B. N. Dev, Carbon **45**, 2659 (2007), and the references therein.
[40]T. E. Doyle and J. R. Dennison, Phys. Rev. B **51**, 196 (1995).
[41]F. Banhart, J. Kotakoski, and A. V. Krasheninnikov, ACS Nano **5**, 26 (2011).
[42]C. Thomsen and S. Reich, Phys. Rev. Lett. **85**, 5214 (2000).
[43]R. Narula and S. Reich, Phys. Rev. B **78**, 165422 (2008).
[44]J. F. Ziegler, J. P. Biersack, U. Littmark, *The Stopping and Range of Ions in Matter* (Pergamon Press, New York, 1995).